Remote Temperature Monitoring of Cells Exposed to Millimeter-Wave Radiation using Microscopic Raman Spectroscopy

Victor Pikov[1] and Peter H. Siegel, *Fellow IEEE*[2*]

[1] Huntington Medical Research Institute, Pasadena, CA 91105 USA
[2] California Institute of Technology, Pasadena, CA 91125 USA

Running title: Thermal Monitoring & Raman Spectroscopy
Keywords: cells, temperature, Raman, microspectroscopy, millimeter-wave, non-invasive, water

Corresponding Author's Address:
Peter H. Siegel
Beckman Institute
MC 139-74
California Institute of Technology
1200 E. California Blvd.
Pasadena, CA 91125.
Email: phs@caltech.edu

Victor Pikov's email: pikov@hotmail.com

* both authors equally contributed to the work

Abstract

A simple setup is demonstrated for remote temperature monitoring of water, water-based media, and cells on a microscopic scale. The technique relies on recording changes in the shape of a stretching band of the hydroxyl group in liquid water at 3100 to 3700 cm^{-1}. Rather than direct measurements in the near-IR, a simple Raman spectrometer setup is realized. The measured Raman shifts are observed at near optical wavelengths using an inverted microscope with standard objectives in contrast to costly near-IR elements. This allows for simultaneous visible inspection through the same optical path. An inexpensive 671 nm diode pump laser (<100mW), standard dichroic and low pass filters, and a commercial 600-1000 nm spectrometer complete the instrument. Temperature changes of 1°C are readily distinguished over a range consistent with cellular processes (25-45°C) using integration times below 10 seconds. Greatly improved sensitivity was obtained by an automated two-peak fitting procedure. When combined with an optical camera, the instrument can be used to monitor changes in cell behavior as a function of temperature without the need for invasive probing. The instrument is very simple to realize, inexpensive compared to traditional Raman spectrometers and IR microscopes, and applicable to a wide range of problems in microthermometry of biological systems. In a first application of its kind the instrument was used to successfully determine the temperature rise of a cluster of H1299 derived human lung cells adhered to polystyrene and immersed in PBS under exposure of RF millimeter wave radiation (60 GHz, 1.3, 2.6 and 5.2 mW/mm^2).

Introduction

The remote measurement of temperature on a microscopic scale has been enabled by the advent of the IR microscope (1). However this instrument is extremely costly (e.g. Thermo Scientific Nicolet^{TM} iN10 infrared microscope is currently priced at $75-100K), and when used for biological measurements, where specimens are often sandwiched between plastic or glass plates or immersed in liquids, the accuracy suffers from differences in emissivity in the various layers that must be penetrated before reaching the sample. It is also difficult to discern the temperature emanating specifically from a cellular or tissue layer immersed in culture medium since water is a very strong IR absorber. Consequently, only the surface temperature has been accurately determined by this type of system. A novel method for remote probing the temperature of liquid water on a microscopic scale was demonstrated recently (2, 3). This technique uses the spectroscopic measurement of the near IR stretching band of water (4), which changes both its absorption amplitude and shape as a function of temperature. The focus of the IR studies was the change in absorption amplitude with temperature using a sample with controlled thickness. Similar to water, the spectral absorption and reflection signatures of assorted biological solutions and tissues exhibited a gradual change with temperature in the near-IR water lines of 960, 1200 and 1400 nm (5). In both studies (4, 5), regression analyses were performed and derived linear models were able to accurately predict the measured temperature change in the tissue for a given variation in spectral absorbance. In the wavenumber range between 3100 and 3700 cm^{-1} (wavelengths from 2.7 to 3.2 μm), the broad Raman band is due to intramolecular vibrational motion of the hydroxyl group of water. Possible vibrational modes include symmetric stretching (ν_1), an overtone of bending ($2\nu_2$), and antisymmetric stretching (ν_3) (6), but experimental studies indicate that only the ν_1 mode is prominent in the Raman measurements (7, 8). The width and multi-peak shape of the ν_1 mode has been attributed to coupling of the hydroxyl group stretching with the energy of intra- and inter-molecular hydrogen bonds (6, 9-11). Formation of these hydrogen bonds can reduce the wavenumber (7) and amplitude (12) of this hydroxyl stretching motion. The band profile has been decomposed into several Gaussian components, possibly indicating the varying number of hydrogen bonds (6) or their strength (weak vs. strong) (11). Different authors identified two (13), three (11, 14), four (6, 15), or even five components (16) in the hydroxyl stretching band, while a recent rigorous analysis of assorted decomposition approaches (17) indicated that a two-component decomposition is adequate for liquid water at temperatures ranging from 5 to 100°C.

This spectral signature of water, although very distinct, falls well into the near-IR region making direct observation through a typical optical system very difficult. However, by employing well-established Raman spectroscopy techniques, it is possible to shift the measured spectrum to the near-visible region of 800-900 nm, which permits the use of standard microscope objectives and filters while avoiding the background bio-fluorescence of the visible spectral region. In this report, we present a very simple instrument arrangement for observing the 3200-3700 cm^{-1} hydroxyl stretching band and show that an accurate estimation of temperature on a microscopic scale can be obtained with short detection time and low pump laser power level, making it compatible with studies of living cells and tissues. In addition we show that a narrow

spectral signature from polystyrene, a common culture dish material, is located near the hydroxyl stretching band and can be used to determine the axial focal plane within the culture dish containing the cells. The method can be used to accurately monitor the temperature of biological specimens in plastic or quartz (but not glass) containers with minimal cost and great flexibility. Both the instrumentation and the initial measurements in biological samples are presented.

Growing interest in the effects of millimeter and submillimeter wave radiation on biological systems, especially cells and cellular processes prompted the first application for the Raman spectrometer in monitoring and calibrating the temperature rise of living cells exposed to strong RF fields. The results of the first experiments performed on direct microscopic observations of the impact of 60 GHz radiation on the temperature of H1299 human derived lung cells adhered to a polystyrene membrane and immersed in PBS are given. In cross comparisons with an IR camera, the measurements validate the superiority of the Raman approach in the non-invasive characterization of temperature at a microscopic scale.

Methods

Microscopic Raman Spectroscopy.

The setup which was used to excite and record the spectrum, is based on a Nikon Diaphot™ inverted microscope with standard 4, 10 and 20X objectives (Fig. 1). The Diaphot model is particularly flexible as it has a very open area above the stage with a retractable illuminator, two output ports plus the binocular eyepieces, an under the turret rear illumination path typically used for epi-fluorescence, and a dichroic filter bay which accepts standard cube filter holders. The rear illumination periscope tube was stripped of its collimating lenses, the front left optical port was fitted with an inexpensive cooled CCD camera (model 3.3MPC, Tucsen Digital Imaging Technology, Fuzhou, China) and the front 35 mm camera port was used to interface to a standard focusing objective (20X) and a multimode optical fiber (diameter 50 μm). The rear illumination lamp tube was removed and the port was fitted with a 671 nm clean up filter (660-680 nm, Omega Optical). A free-space DPSS 671 nm 200mW diode laser (model VA-I-N-671, Beijing Viasho Technology, Beijing, China) was optically guided by a folding mirror into the rear illumination tube where the nearly collimated beam passes laterally into the filter cube and then bounced upward by a 45° flat made up of a 700 nm long-wavelength-pass dichroic filter (High Efficiency Cold Mirror, Navitar Coating Labs, Newport Beach, CA). The laser light is then routed through the objective turret and focused onto the plane of the sample stage. The laser was set at a constant current of 2.0 A, yielding 300 mW of power at the laser output, which was reduced to approximately 70 mW at the sample plane after passing through the folding mirror, cleanup filter, turret glass, dichroic cube filter, and 20X objective lens.

The backscattered Raman light was captured collimated by a 20X objective, filtered from the backscattered Rayleigh light by the dichroic mirror in the filter cube, and, following the microscope optical path, directed forward to the 35 mm camera port where it was apertured by the film cutout built into the microscope. The beam was then passed through a long-wavelength-pass filter (> 785 nm, BLP01-785R-25, Semrock) to further block the backscattered Rayleigh light and any stray laser light from the sample that passed through the dichroic mirror. Finally,

the beam was refocused by a 20X objective onto a multimode fiber with a standard SMA connector. The fiber was centered on the beam using a fiber launch positioning jig (model MBT612, Thorlabs). The fiber was coupled into a spectrometer (Shamrock SR-163, Andor) with cooled electron-multiplying CCD (iDUS DV420A, Andor) through a standard fiber line collimator and no additional coupling slit. A photo of the entire system is shown in Fig. 2.

To assure that the laser pump and optical path to the spectrometer and CCD ports overlapped exactly, the pump laser focal spot was co-aligned with the top illuminator by adjustments to the laser position and angle and the collinear red and white spots verified in the CCD camera (Fig. 3). Note that the laser spot diameter determines the primary area sampled in the spectrometer as all the backscattered energy from this region was collected and focused onto the optical fiber by the second 20X objective at the camera port. The spectrometer was used to peak up the Raman signal from the water sample through adjustments of the objective-to-fiber coupling stage as well as optimization of the position of the objective within the slightly larger camera port aperture.

Using the aforementioned filters and the Andor SR-163 spectrometer with 300 lines/mm grating, the transmitted range of backscattered Raman light was between 800 and 1020 nm with 0.8 nm resolution. Employing the 671 nm laser pump, the 3200-3500 cm^{-1} vibrational water peaks appear between 855 and 880 nm. An added bonus is the presence of two strong and relatively narrow Raman shifted peaks of polystyrene at ~3140 cm^{-1} that appear at 850 nm and were present in the Corning and Falcon plastic Petri dishes as well as in an enclosed thickness-controlled and gas-permeable cell culture dish (Nunc OptiCell™ Culture System, BioCrystal Ltd.), but not in a glass slide, glass cover slip, or quartz glass (Fig. 4). The polystyrene peak fell directly outside the water spectrum and can be used to determine the axial focal plane of the pump laser. This line appears as the focal plane of the objective passes through the plastic. An additional benefit of the OptiCell dish is having both a top and bottom plastic membrane (spaced 2 mm apart), which demarcates a scan through the internal liquid sample by the appearance, disappearance and reappearance of the polystyrene Raman peaks (Fig. 5 and Supplementary Material, Fig. S1).

The appearance of the two polystyrene peaks at 850 nm was evident even at 0.5-second-long integration time in the spectrometer and could be used to quickly calibrate the focus wheel of the microscope as well as peaking up the overall signal. Depending on the location of the attached cells at the top or bottom membrane of the Opticell dish, the focal plane of the microscope could then be precisely adjusted for measuring the Raman signal from the cells rather than the adjacent medium. The integration time of the spectrometer was then set to 8 seconds per measurement to improve the signal-to-noise ratio of the collected data.

Temperature measurement and controlled general heating.

The configuration, depicted in Fig. 6, was employed to measure the Raman spectra in the 800-1020 nm range of various samples of de-ionized (DI) water and water-based culture media as a function of temperature. In each case 10 ml of solution was injected into an OptiCell dish and all air bubbles were removed to leave a uniform 2 mm-thick fluid sample sandwiched between the 75 µm-thick treated polystyrene membranes. In order to accurately measure the temperature of the fluid in the region directly around the illuminated sample, two separate independent monitors

were set up. A non-contact thermal IR imaging camera with 0.1°C discrimination (Inframetrics Thermacam PM290, FLIR Systems) was positioned above the sample stage and continually recorded the sample temperature over an approximate area of 1.5x1.5 cm at a resolution of ~50x50 µm. This camera allowed us to monitor the uniformity of the temperature changes over a wide region around the sample. As an absolute monitor of the fluid temperature inside the OptiCell and directly adjacent to the field of view, a miniature coaxial Type T thermocouple probe with 0.6 mm-diameter sampling tip, 0.1 second time constant, and 0.1°C accuracy (IT-18, Physitemp, Clifton, New Jersey) was inserted into the OptiCell holder through a 22 gauge needle and positioned immediately outside the viewing circle of the 20X microscope objective (marked on the plastic with a felt tip pen) (Fig. 7). The OptiCell dish with the inserted thermocouple was air sealed using a small dab of Polydent around the needle entry point, bridging the thermocouple wires, but allowing easy removal for later use. Between the thermocouple and the IR camera the region being directly illuminated by the pump laser and imaged through the CCD and camera (spectrometer) ports could be continuously monitored.

Due to the small volume (10 ml) and large area (50 cm^2) of the OptiCell dish, it was extremely simple to slowly heat (or cool) the entire sample with a small hair dryer and fan. During data collection, the hair dryer was used to flow warm air across the surface of the cell and the IR camera was used to make sure the area around the sample spot stayed at a uniform temperature while the thermocouple measured the absolute temperature of the fluid itself, just outside of the laser illumination circle. The measurements were then repeated during a cooling cycle. For the temperatures approaching ambient, a small fan was used to speed up the cooling by increasing air convection. During all temperature manipulations (both heating and cooling), the temperature change was considerably slower (0.5°C per minute) than the integration time of the spectrometer (8 seconds).

Focal heating using RF millimeter wave exposure system.

One practical use of the remote focal thermal monitoring in our laboratory was related to monitoring temperature changes in cell cultures during exposure to high frequency RF radiation (millimeter and submillimeter waves, frequencies between 60 and 600 GHz). As the application of these relatively untapped spectral bands expands into the areas of communications, imaging and security, there is a growing need to understand what, if any, impact this penetrating radiation has on cellular processes. One measure of such impact is the change in temperature induced in cell cultures and tissues. Measuring such changes during and after RF exposure at a microscopic level is extremely difficult. As mentioned earlier, thermal IR cameras and microscopes tend to measure only the surface temperature, especially in water-based media. If the cells reside at the bottom of a media container it may be impossible to accurately record any temperature rise on this layer using standard IR techniques. The Raman scattering measurements described in this paper allow one to position the axial focal spot at any point within the (relatively small) volume of the culture dish. It makes it simple with such a system to illuminate the cells with RF energy from the top (Fig. 2, center) while monitoring the temperature and any visible changes in the cells via the bottom, using the normal viewport of an inverted microscope.

The setup for RF exposure is shown in Fig. 2, with a close-up of the microscope stage area in the inset. A millimeter wave generator consisting of a commercial 50-75 GHz swept frequency

backward wave oscillator (BWO, formerly Micronow model 705 sweeper with a Siemens RWO-50 tube, similar units now available from Elva-1, St. Petersburg, Russia) was used to inject RF power through a series of waveguide components that terminate and hence radiate directly onto the top of the Opticell polystyrene membrane. The polystyrene has very low RF loss and the WR-15 waveguide (1.9x3.8mm aperture) is loaded with a tapered PTFE wedge to match the power into the plastic with only minor reflections. The cells were adhered to the top of the container and thus were directly impacted by the RF energy before it could be absorbed by surrounding culture medium. The RF power and absolute frequency from the millimeter wave generator were measured directly using calibrated detectors that are switched into the RF path and the power incident on the OptiCell is inferred by measuring the losses through the extra waveguide between the switch and the sample. An in-line calibrated attenuator is used to vary the incident power in known steps.

Measurements consisted of placing a large cell cluster directly under the RF waveguide and applying fixed frequency (60 GHz) calibrated RF power to the OptiCell for a fixed period of time (~4 minutes) until the temperature rise in the surrounding medium reached an equilibrium, as measured by the IR camera. The highest power level was applied first and the cells were allowed to cool for several minutes before the next exposure. The IR camera cannot view, and hence measure, the temperature directly under the waveguide, where the power output is peaked, because the metal guide hides this region from a top view. The camera can only record the temperature directly surrounding the metal waveguide aperture (~2 mm from the center illumination hot spot). However the Raman signal is collected from below and is easily tagged directly to the center of the cell field. The RF output from the waveguide aperture roughly follows a Gaussian power distribution which rolls off from the center of the field in an approximately spherical pattern. Little or no power penetrates through to the bottom of the OptiCell as the PBS is extremely absorbing at this frequency.

The cell culture was exposed to three levels of RF power (~3.6, 7.2 and 14.4 mW at the waveguide output port) which varies little over the field of view (~1mm^2) produced by the 20X objective. This power is spread over an area of approximately 2.8mm^2 (set by the waveguide aperture and frequency) giving a maximum power density of ~5.2 mW/mm^2 for the exposure at 14.4 mW. Note that this power level is much greater than the suggested safe limit for long term human exposure of 0.1 mW/mm^2. The Raman spectra were recorded as the temperature was measured by the IR camera in the region directly outside the waveguide aperture. Several cell locations were examined in the culture dish (OptiCell), making it impractical to include a separate microthermocouple probe near each exposure area.

Cell culture.

The H1299 immortalized epithelial cell line is derived from human lung carcinoma and was a gift from Dr. Alex Sigal (Caltech, Pasadena, CA). This cell line is characterized by rather large cells that strongly adhere to all tested plastic surfaces, including those of the Petri dishes and of the OptiCell thin-membrane dish and is the major reason for choosing this particular line for our early investigations (Fig. 7). The cells were grown in RPMI-1640 medium, supplemented with 10% (v/v) fetal bovine serum and 2 mM L-glutamine, in a 5% CO_2 incubator set at a 37°C. For spectroscopy measurements, RPMI was replaced with phosphate-buffered saline (PBS, pH 7.4).

As a possible substitution for PBS, we also evaluated Opti-MEM™ (Invitrogen, Carlsbad, CA), as it exhibits the best optical transparency among the Phenol red-containing media. Opti-MEM is a modification of Eagle's Minimal Essential Medium with a reduced amount of Phenol red (1.1 mg/l) as compared to the standard Dulbecco's modified Eagle's medium (15mg/l).

RESULTS

Raman hydroxyl band in different culture media.

Measurements of the Raman spectrum were made in DI water, PBS, Opti-MEM with Phenol red, Opti-MEM without Phenol red, and a confluent layer of cells in PBS. In all cases, a 20X objective was used. The focal spot being sampled by the Raman spectrometer was approximately 1 mm in diameter. The laser power was 70 mW and the spectrometer integration time was 8 sec. A background count with the laser off was used for subtraction of the CCD dark current and read-out noise. A typical set of spectra are shown in Fig. 8 at a single temperature (25°C). The amplitude of the Raman hydroxyl band varied among the media tested, with the highest intensity seen in the Opti-MEM medium with Phenol red. The amplitude of the Raman hydroxyl band signal was lower in cells than in water or water based media, in concordance with another study (18). No discernable difference was observed in the shape of the hydroxyl band among the various media, DI water, and cells. Due to their lower background intensities as compared with the Phenol red-containing culture medium, we selected the DI water and PBS for the subsequent heating studies.

Analysis of the shape of the Raman hydroxyl band in water and cells during uniform heating.

The Raman signal at the hydroxyl band was collected at gradually increasing and decreasing temperatures in the physiological range of 25 to 45°C as measured by the thermocouple. Changes in the shape of the Raman hydroxyl band was remarkably similar for the DI water (Fig. 9) and cells in PBS (Fig. 10). In addition to point-sampling of the temperature inside the Opticell dish, spatial distribution of the temperature was assessed by an IR camera. It showed a uniform temperature (within 0.2°C) on top of the Opticell dish over a large area surrounding the illumination circle. However, the absolute temperature values, measured by the IR camera, varied by as much as 0.8°C as compared with the thermocouple reading. For this reason, only the thermocouple readings were used for correlation with the Raman changes in this study.

Prior to the peak-fitting analysis, the Raman spectrum data were normalized based on the isosbestic point of the Raman hydroxyl band, found to be at 3440 cm^{-1}. The isosbestic point refers to the wavenumber at which spectra, taken at different conditions (e.g. temperatures, pressures, potentials), cross, putatively due to the equilibrium between the hydrogen-bonded and non-hydrogen-bonded hydroxyl species (19, 20). The isosbestic point value is this study is well within the determined 3400-3500 cm^{-1} range for the liquid water under different polarization conditions (9, 19).

For the analysis of the shape of Raman hydroxyl band, we decided to apply an automated double-peak fitting procedure that does not impose any *a priori* restrictions on the shape or location of the peaks. We used the Fityk program (http://www.unipress.waw.pl/fityk/), which

included three options for automated nonlinear optimization of the double-peak fitting: Levenberg-Marquardt, Nelder-Mead simplex, and the Genetic Algorithm. Of these, Levenberg-Marquardt produced the most consistent results due to avoidance of local minima. We have evaluated several peak functions, including the Gaussian, Lorentzian, Pearson VII, and approximated Voigt/Faddeeva (a convolution of Gaussian and Lorentzian functions). Of these, the approximated Voigt/Faddeeva function (21) proved to be the most robust. Based on initial evaluation, we decided to use the Levenberg-Marquardt optimization method and the approximated Voigt/Faddeeva function for the automated double-peak fitting in this study.

Peak fitting was initially performed for the water Raman spectrum at the 25.2°C nominal temperature (Figure 11). To facilitate the comparison between the peaks, we chose the option for fitting both peaks with functions of the same shape, but let the program to choose the actual optimal shape. In the subsequent peak fittings for the water and cellular spectra at higher temperatures, we kept the wavenumber values of both peaks (3289 and 3518 cm^{-1}) and the shapes of the peaks (-21.32) constant, so that the only variables in the peak fitting were the height and width of the peaks. Area under the peaks was a product of these variables. The ratio of areas under peak 2 versus peak 1 indicated the temperature-dependant expansion of peak 2 relative to peak 1 (Figure 12). Linear regression analysis showed that the ratio of the two spectral peak regions provides an accuracy of at least 1°C. Higher accuracy would be possible with a more sensitive spectrometer. Peak 2/1 area ratio for the cells was significant larger than that for the DI water, as calculated by a paired t-test ($p < 0.001$), while the slope of both regression lines was practically identical (0.0294 for water and 0.0303 for cells).

Analysis of the shape of the Raman hydroxyl band in water and cells during RF heating with millimeter waves.

In this experiment, the cells in PBS were locally heated by RF millimeter wave energy using a metal waveguide matched to, and directly in contact with, the upper polystyrene membrane of the OptiCell. The thermocouple probe could not be used in this setup, as it could not be easily positioned within the OptiCell and would perturb the cell attachment. It is also likely that the readings of the thermocouple would have been affected by direct coupling of the RF radiation to the metal sensing element (although this was not tested explicitly). Therefore, prior to the millimeter wave exposure, a baseline reading of the uniform temperature at the top Opticell surface was taken by the IR camera while the waveguide was lifted off the surface. During RF exposure, the IR camera could no longer read the temperature directly from the irradiated area as it was shadowed by the waveguide aperture (see Fig. 2 inset). Readings were instead taken at the hottest spot immediately adjacent to the waveguide. These IR camera readings, which were expected to be somewhat lower than the temperature directly under the exposure port, were compared with remote temperature measurements obtained by our microscopic Raman spectroscopy technique. Calibration of the Raman readings to an absolute temperature value was done by correlating the baseline IR camera reading with the Raman peak 2/1 area ratio with no RF present. The temperature values during exposure to three levels of millimeter waves (3.6, 7.2 and 14.4 mW) were calculated using the slope value of 0.03 obtained in the earlier calibration experiment with PBS (Figure 13, black dots). Between each millimeter wave exposure, the cells in the Opticell dish were cooled until they reached the baseline temperature, as measured by the IR camera. The Raman-based temperature readings during the exposure were consistently higher

than the IR camera readings (Figure 13, white dots), confirming our ability to measure actual focal plane heating without direct visual or thermocouple access in a microscopic region. The considerable millimeter wave-induced heating (~4°C), observed in the cells during the RF exposure at 14.4 mW, can be contrasted with a lack of any detectable heating in the cells during exposure to 70 mW of laser light at 671 nm as measured by the thermocouple. This highlights the dramatic difference in absorption by water at the two wavelengths.

DISCUSSION

The present study describes the setup and use of a simple, low-cost, flexible Raman spectrometer system for remote measurement of the temperature in water-based media on a microscopic scale. The absolute temperature can be inferred from a ratiometric evaluation of dual peaks in the Raman hydroxyl band at the 3200-3700 cm^{-1}. The measured Raman spectrum falls into the region of 800-900 nm, permitting the use of standard microscope objectives and optical filters, a low-cost optical pump laser, and a convenient fiber-coupled spectrometer with a standard CCD, not optimized for the near-IR. The most expensive part of the measurement system is the spectrometer which costs between $10K and $15K. The microscope, laser, filters and fiber were obtained for under $10K total. The use of the 800-900 nm band significantly reduces the background noise from fluorescence inherent to biological samples. The described setup has been used to measure the temperature dependence of DI water and cells in PBS. Temperature accuracy of 1°C has been attained with 8-sec sampling by employing an automated nonlinear optimization method for double-peak fitting in the Raman hydroxyl band. The technique should prove useful for monitoring temperature changes in culture media without the need for direct thermocouple probing and through common culture plates composed of polystyrene or quartz. The use of plastic dishes provides the added advantage of being able to visualize a narrow spectral signature from polystyrene near the hydroxyl stretching band (at 850 nm) that can be used to accurately (within the NA of the objective) determine the axial focal plane in the culture dish. The strength of the Raman polystyrene signal allows short measurement times (less than 1 sec) for fast and precise focusing and alignment of the spectroscopic optical elements. Phenol red-containing medium should be avoided during the spectrometric temperature measurements due to its high fluorescence background, reducing the signal-to-noise ratio at the Raman hydroxyl band. However, minimal background fluorescence was observed in Phenol red-free culture medium and PBS.

The instrument was used to record, for the first time, the direct rise in temperature of a cluster of cells adhered to a polystyrene membrane and immersed in PBS, under direct exposure to millimeter wave radiation. The technique successfully recorded a significant temperature difference in the region directly under the RF beam, from that of the nearest accessible region (viewed by an IR camera) which lay directly outside the exposure area. In addition, by calibrating the axial focal spot of the objective lens with the Raman peaks it was possible to measure the temperature at the plane of the cells and through 2mm of PBS solution. The authors believe these are the very first measurements of this type and lay the groundwork for much more extensive investigations of the impact of RF radiation on cells and cell processes.

In a similar fashion, this setup can be used to monitor thermal changes on the micron scale associated with local application of drugs, affecting thermoplastic cellular functions (e.g. metabolism).

In summary, we have described a simple inexpensive method for quick, precise and reliable remote microscopic measurement of cellular temperature inside the culture medium that is applicable to a wide range of problems in microthermometry of biological systems.

ACKNOWLEDGEMENTS

The authors gratefully acknowledge the contributions of Ms. Kathleen Teves, a summer undergraduate research assistant from UC Irvine, in collecting the measurements data and the continuing support of Caltech Professors David B. Rutledge and Scott E. Fraser. They also thank Dr. Alex Sigel for the H1299 cell line and they especially thank Mr. Jay Moskovic for the loan of the Andor spectrometer. This work was carried out under grants from the National Institutes of Health.

REFERENCES

1. **Roush, P. B., editor. 1987. The Design, Sample Handling, and Applications of Infrared Microscopes. ASTM Intl**
2. **Kakuta, N., F. Li, and Y. Yamada. 2005. A method for measurement of water temperature in micro-region using near infrared light. In 27th IEEE-EMBS. 3145-3148.**
3. **Kakuta, N., H. Arimoto, H. Momoki, F. Li, and Y. Yamada. 2008. Temperature measurements of turbid aqueous solutions using near-infrared spectroscopy. Appl. Opt. 47:2227-2233.**
4. **Hollis, V. S., T. Binzoni, and D. T. Delpy. 2001. Noninvasive monitoring of brain tissue temperature by near-infrared spectroscopy. In Optical Tomography and Spectroscopy of Tissue IV. Proc. SPIE. 470-481.**
5. **Kelly, J. J., K. A. Kelly, and C. H. Barlow. 1995. Tissue temperature by near-infrared spectroscopy. In Optical Tomography, Photon Migration, and Spectroscopy of Tissue and Model Media: Theory, Human Studies, and Instrumentation. Proc. SPIE. 818-828.**
6. **Rice, S. A. 1975. Conjectures on the structure of amorphous solid and liquid water. Top Curr Chem:109-200.**
7. **Libowitzky, E. 1999. Correlation of O-H stretching frequencies and O-H center dot center dot center dot O hydrogen bond lengths in minerals. Monatsh Chem 130:1047-1059.**
8. **Simonelli, D., and M. J. Shultz. 2001. Temperature dependence for the relative raman cross section of the ammonia/water complex. J Mol Spectrosc 205:221-226.**
9. **Walrafen, G. E., M. R. Fisher, M. S. Hokmabadi, and W. H. Yang. 1986. Temperature dependence of the low- and high-frequency Raman scattering from liquid water. J Chem Phys 85:6970-6982.**
10. **Green, J. L., A. R. Lacey, and M. G. Sceats. 1986. Spectroscopic evidence for spatial correlations of hydrogen bonds in liquid water. J Phys Chem 90:3958-3964.**
11. **Pershin, S. M., A. F. Bunkin, V. A. Lukyanchenko, and R. R. Nigmatullin. 2007. Detection of the OH band fine structure in liquid water by means of new treatment procedure based on the statistics of the fractional moments. Laser Phys Lett 4:809-813.**
12. **Lutz, H. D. 2003. Structure and strength of hydrogen bonds in inorganic solids. J. Mol. Struct. 646:227-236.**
13. **Risovic, D., and K. Furic. 2005. Comparison of Raman spectroscopic methods for the determination of supercooled and liquid water temperature. J Raman Spectrosc 36:771-776.**
14. **Brubach, J. B., A. Mermet, A. Filabozzi, A. Gerschel, and P. Roy. 2005. Signatures of the hydrogen bonding in the infrared bands of water. J Chem Phys 122:184509.**
15. **Walrafen, G. E., W. H. Yang, Y. C. Chu, and M. S. Hokmabadi. 1996. Raman OD-Stretching Overtone Spectra from Liquid D2O between 22 and 152 degrees C. J Phys Chem 100:1381-1391.**
16. **Carey, D., M. , and G. Korenowski, M. . 1998. Measurement of the Raman spectrum of liquid water. J Chem Phys 108:2669-2675.**
17. **Smith, J. D., C. D. Cappa, K. R. Wilson, R. C. Cohen, P. L. Geissler, and R. J. Saykally. 2005. Unified description of temperature-dependent hydrogen-bond rearrangements in liquid water. Proc Natl Acad Sci U S A 102:14171-14174.**
18. **Thompson, S. A., F. J. Andrade, and F. A. Inon. 2004. Light emission diode water thermometer: a low-cost and noninvasive strategy for monitoring temperature in aqueous solutions. Appl Spectrosc 58:344-348.**
19. **Walrafen, G. E., M. S. Hokmabadi, and W. H. Yang. 1986. Raman isosbestic points from liquid water. J Chem Phys 85:6964-6969.**
20. **Geissler, P. L. 2005. Temperature dependence of inhomogeneous broadening: on the meaning of isosbestic points. J Am Chem Soc 127:14930-14935.**
21. **Wells, R. J. 1999. Rapid approximation to the Voigt/Faddeeva function and its derivatives. J Quant Spect Radiat Trans 62:29-48.**

Figure legends

Fig. 1. Block diagram of the Diaphot microscope setup and optical paths.

Fig. 2. Photo of instrument setup showing pump laser, IR monitor camera, thermocouple monitor, OptiCell culture dish, camera port fiber coupler, spectrometer and millimeter wave exposure system with the waveguide output on top of the biosample.

Fig. 3. CCD picture through eyepiece showing co-aligned 671nm laser light spot and top white light illumination spot on one mm diameter circle drawn on a piece of ground glass positioned at the objective focus. The dark rim around the edge of the field is the out of focus aperture of the white light illuminator used to center the illuminator over the field of view.

Fig. 4. Raman spectra of polystyrene-based culture dishes, glass and quartz. The 850 nm peak is present in Corning™ (430166), Falcon™ (25369-022), and VWR™ (25384-302) Petri dishes as well as in OptiCell™ dishes. Glass samples, such as a 1 mm-thick glass slide (48300-025, VWR) and 0.15 µm-thick cover slip (48366-067, VWR) were highly fluorescent, while 1 mm-thick quartz glass was remarkably opaque.

Fig. 5. Raman spectra showing progression of focal plane from the bottom, through 2 mm of water, and to the top of OptiCell dish.

Fig. 6. Photo of the OptiCell dish filled with DI water with the inserted coaxial thermocouple probe sitting next to the area to be illuminated and spectrally imaged (black circle, 1 mm in diameter). The clear area is 75x65 mm. The fluid thickness is 2 mm and the top and bottom polystyrene films are 75 µm thick.

Fig. 7. Microphotograph of H1299 cells adhered to the OptiCell membrane, taken through the CCD camera port with a 20X objective. The black circle (1 mm in diameter) is marked on the membrane for subsequent localization of the cells for time-lapse imaging.

Fig. 8. Raman spectra of various water-based media inside the OptiCell dish at 25°C. Although changes in total signal are apparent due to the amount of Raman backscatter, the spectral line shape is very consistent.

Fig. 9. Temperature dependence of Raman spectrum in DI water between 25.2 and 44.2°C at 1°C intervals. All data is collected from the same position on the OptiCell dish and referenced against the in-situ thermocouple. The pump laser was focused approximately in the middle of the 2 mm-thick sample.

Fig. 10. Temperature dependence of Raman spectrum in H1299 immortalized epithelial cell line between 25.2 and 44.2°C at 1°C intervals. The cells were cultured in RPMI medium in OptiCell dish at 37°C and 5% CO2. For spectroscopy measurement, the RPMI was replaced with PBS.

Fig. 11. Double-peak fitting of the OH stretching band at a temperature of 25.2°C on a 2 mm thick sample of DI water in an OptiCell dish. The peak functions are the approximated Voigt/Faddeeva (a convolution of Gaussian and Lorentzian functions). Both peaks were specified to have the same shape, allowing the common shape and individual center wavenumbers, heights and widths of the peaks to be varied using an automated Levenberg-Marquardt optimization method for double-peak fitting. For the subsequent peak fittings at higher temperatures, the shape of the peaks and the peak center wavenumbers were kept constant.

Fig. 12. Ratio of the areas under peak 2 versus peak 1 of the OH stretching Raman band at temperatures between 25.2 and 44.2°C of DI water (outlined circles) and H1299 cells in PBS (solid triangles) in an OptiCell dish. Linear regression for the DI water data (R^2 = 0.996) is shown as a dotted line and for the H1299 cells (R^2 = 0.990) – as a solid line. Inset shows a close-up view of the Opticell dish with the laser light coming in from below and millimeter wave waveguide aperture above.

Fig. 13. Ratio of the areas under peak 2 versus peak 1 of the OH stretching Raman band during RF heating with three levels of millimeter wave power (3.6, 7.2, and 14.4 mW) introduced via a matched WR-15 waveguide aperture (1.88x3.76mm). The white circles indicate the temperature measurements immediately adjacent to the waveguide, but well outside the field of view, taken with the IR camera, while the black circles indicate the calculated temperature values directly under the center of the waveguide and not visible in the camera. The calculated points are derived from the baseline IR camera reading (no waveguide present) and the slope of 0.03 measured with the thermocouple and heater on an identically configured OptiCell. At the baseline reading, the white and black circles are overlapped.

Fig. S1. (Supplemental). Short movie showing the rise and fall of the distinct spectral signatures of polystyrene and water as the axial focal position of the 20X objective is varied. This allows precise calibration of the focal plane from which the temperature readings are derived.

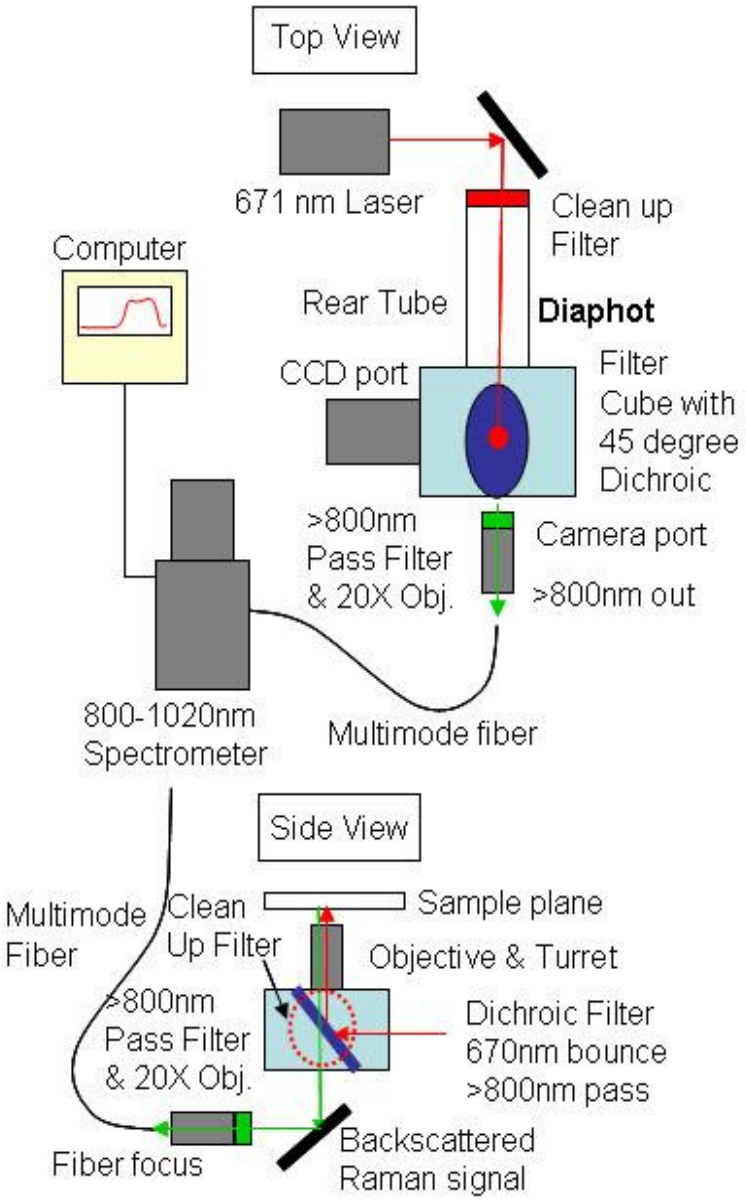
Top View
671 nm Laser
Clean up
Filter
Computer
Rear Tube
Diaphot
CCD port
Filter
Cube with
45 degree
Dichroic
>800nm
Pass Filter
& 20X Obj.
Camera port
>800nm out
800-1020nm
Spectrometer
Multimode fiber
Side View
Multimode
Fiber
Clean
Up Filter
Sample plane
Objective & Turret
>800nm
Pass Filter
& 20X Obj.
Dichroic Filter
670nm bounce
>800nm pass
Fiber focus
Backscattered
Raman signal

Fig. 1.

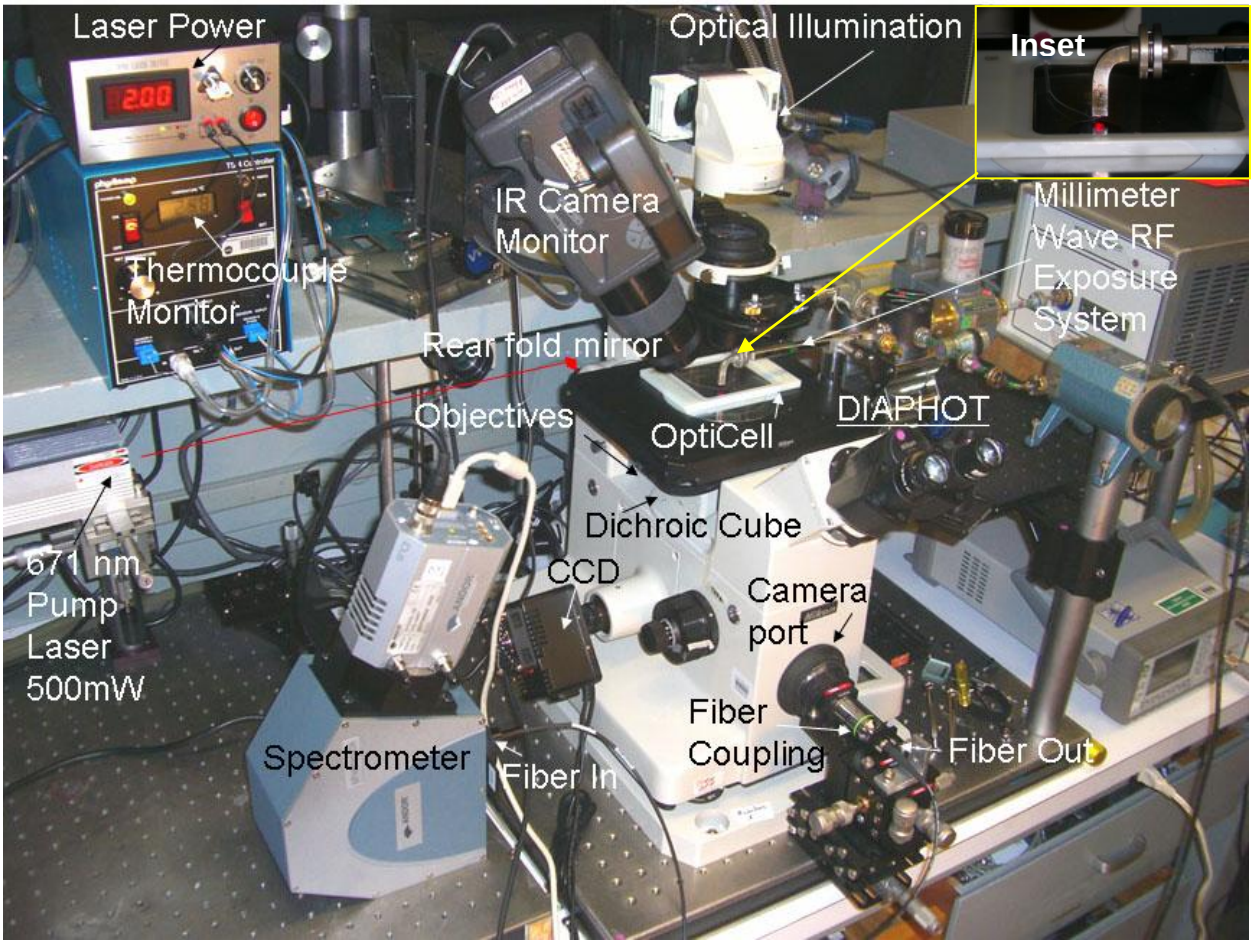
Laser Power
Optical Illumination
Inset
IR Camera Monitor
Millimeter Wave RF Exposure System
Thermocouple Monitor
Rear fold mirror
Objectives
OptiCell
DIAPHOT
Dichroic Cube
671 nm Pump Laser 500mW
CCD
Camera port
Fiber Coupling
Fiber Out
Spectrometer
Fiber In

Fig. 2.

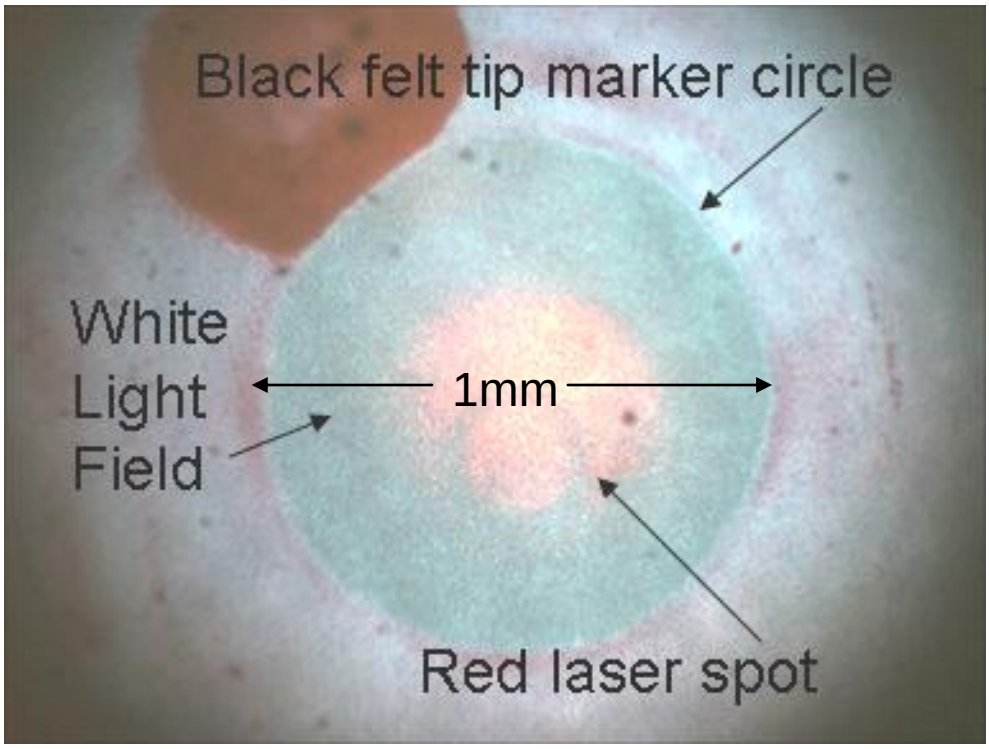
Black felt tip marker circle
White
Light
Field
1mm
Red laser spot

Fig. 3.

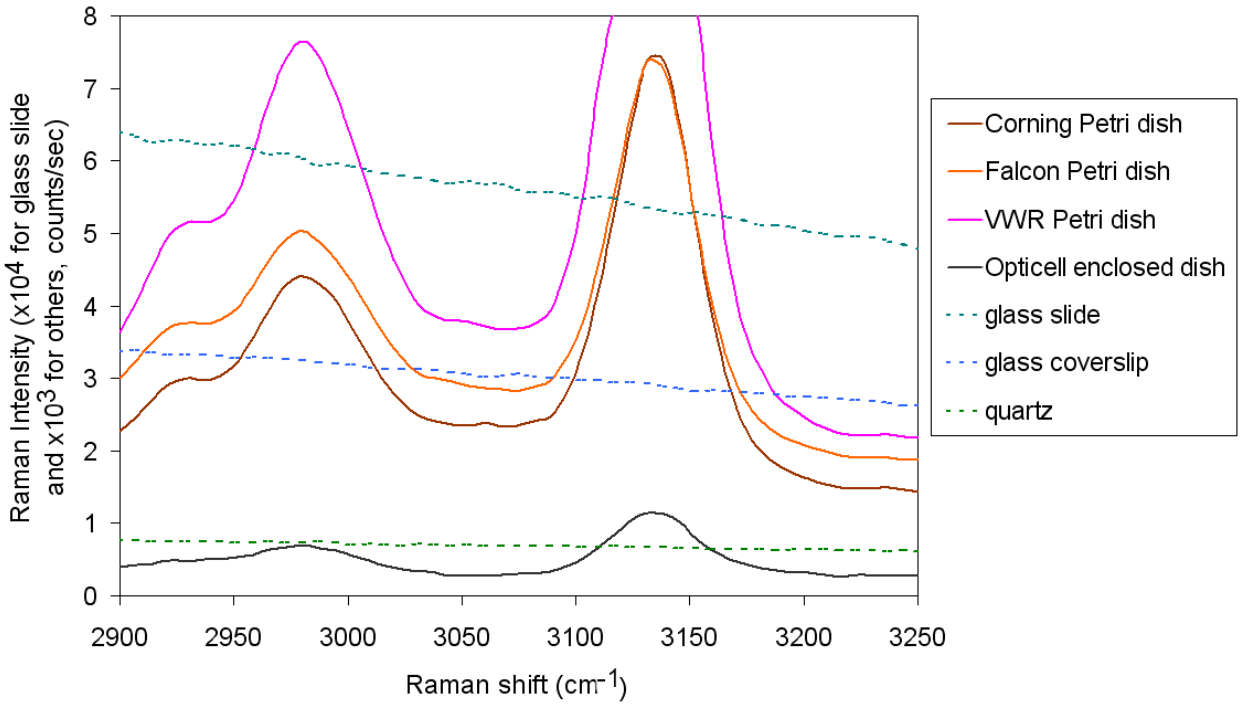
Raman Intensity (x10^4 for glass slide and x10^3 for others, counts/sec)
Raman shift (cm^-1)
0
1
2
3
4
5
6
7
8
2900
2950
3000
3050
3100
3150
3200
3250
Corning Petri dish
Falcon Petri dish
VWR Petri dish
Opticell enclosed dish
glass slide
glass coverslip
quartz

Fig. 4.

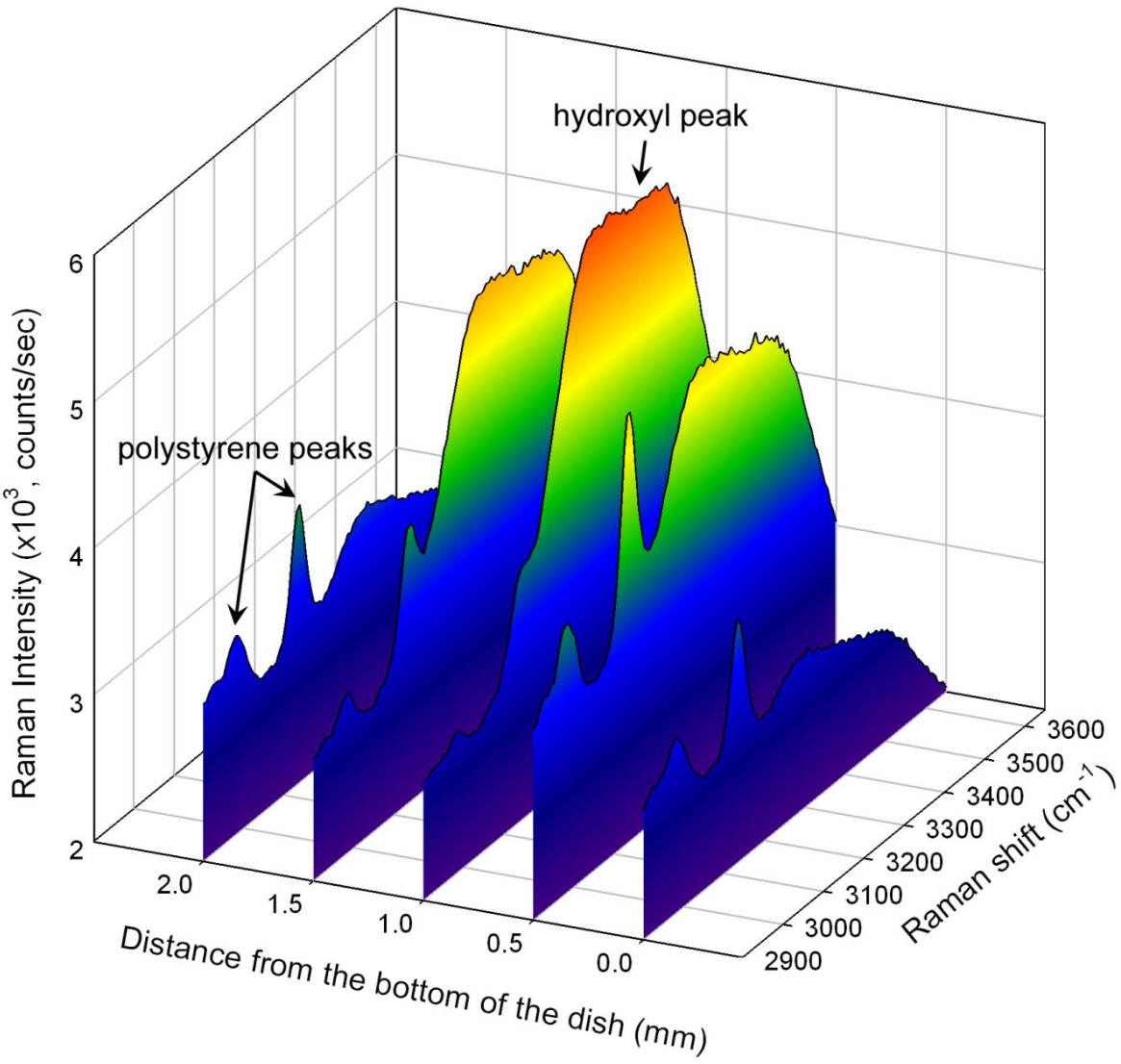
hydroxyl peak
polystyrene peaks
Raman Intensity (x10^3, counts/sec)
6
5
4
3
2
2.0
1.5
1.0
0.5
0.0
Distance from the bottom of the dish (mm)
3600
3500
3400
3300
3200
3100
3000
2900
Raman shift (cm^{-1})

Fig. 5.

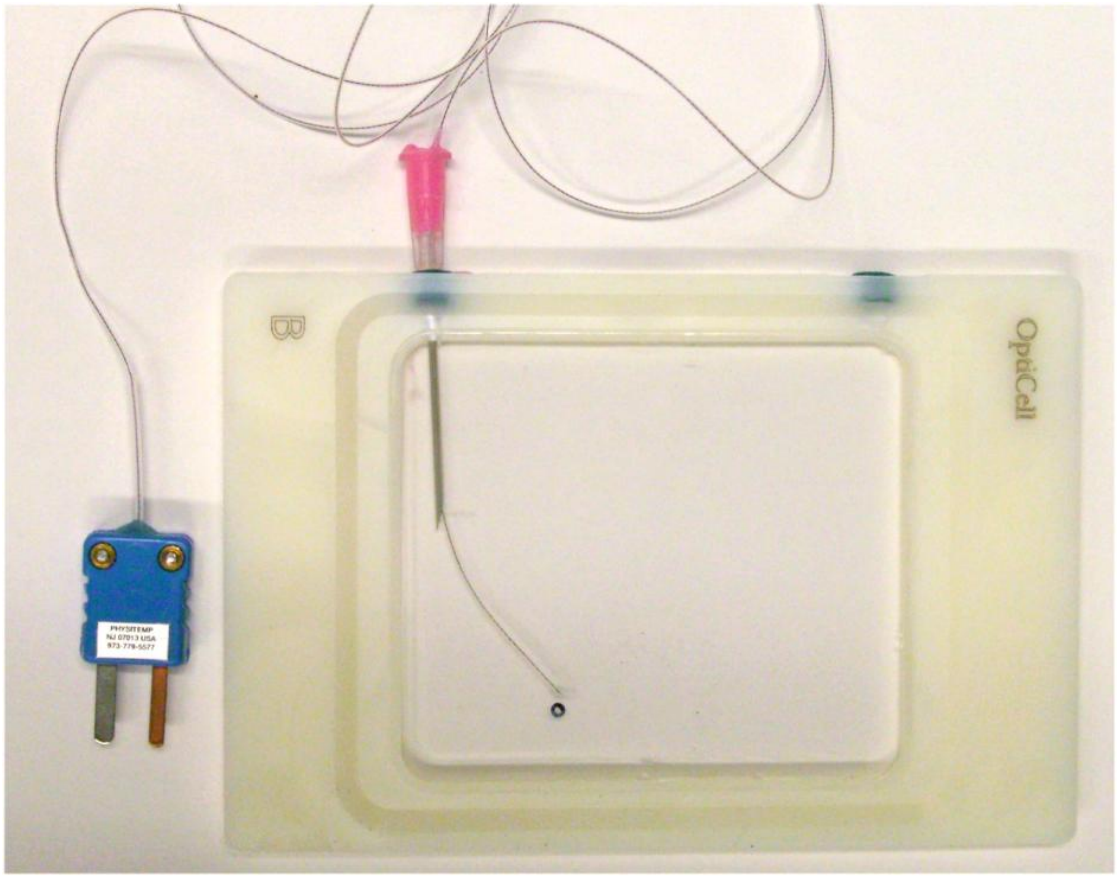

Fig. 6.

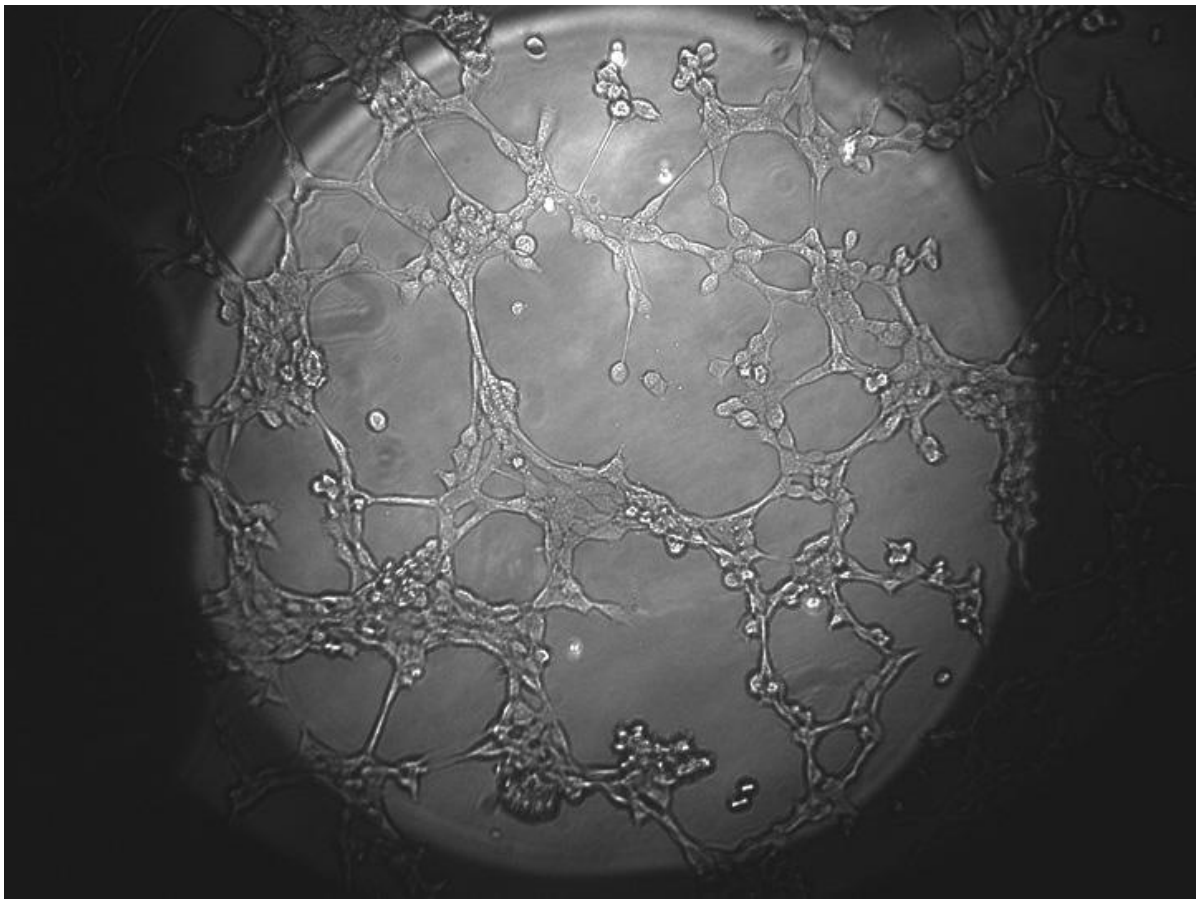

Fig. 7.

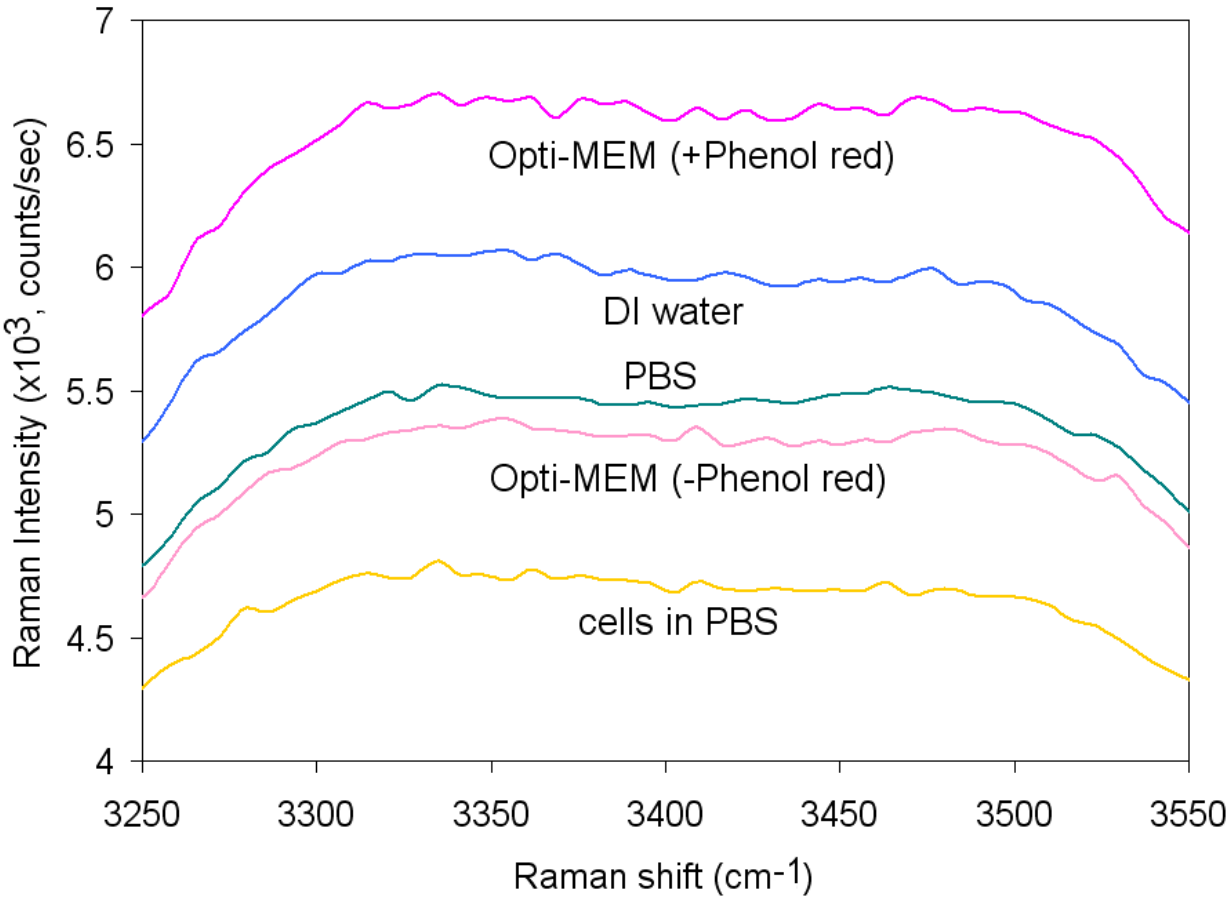
Raman Intensity (x10^3, counts/sec)
7
6.5
6
5.5
5
4.5
4
3250
3300
3350
3400
3450
3500
3550
Raman shift (cm-1)
Opti-MEM (+Phenol red)
DI water
PBS
Opti-MEM (-Phenol red)
cells in PBS

Fig. 8.

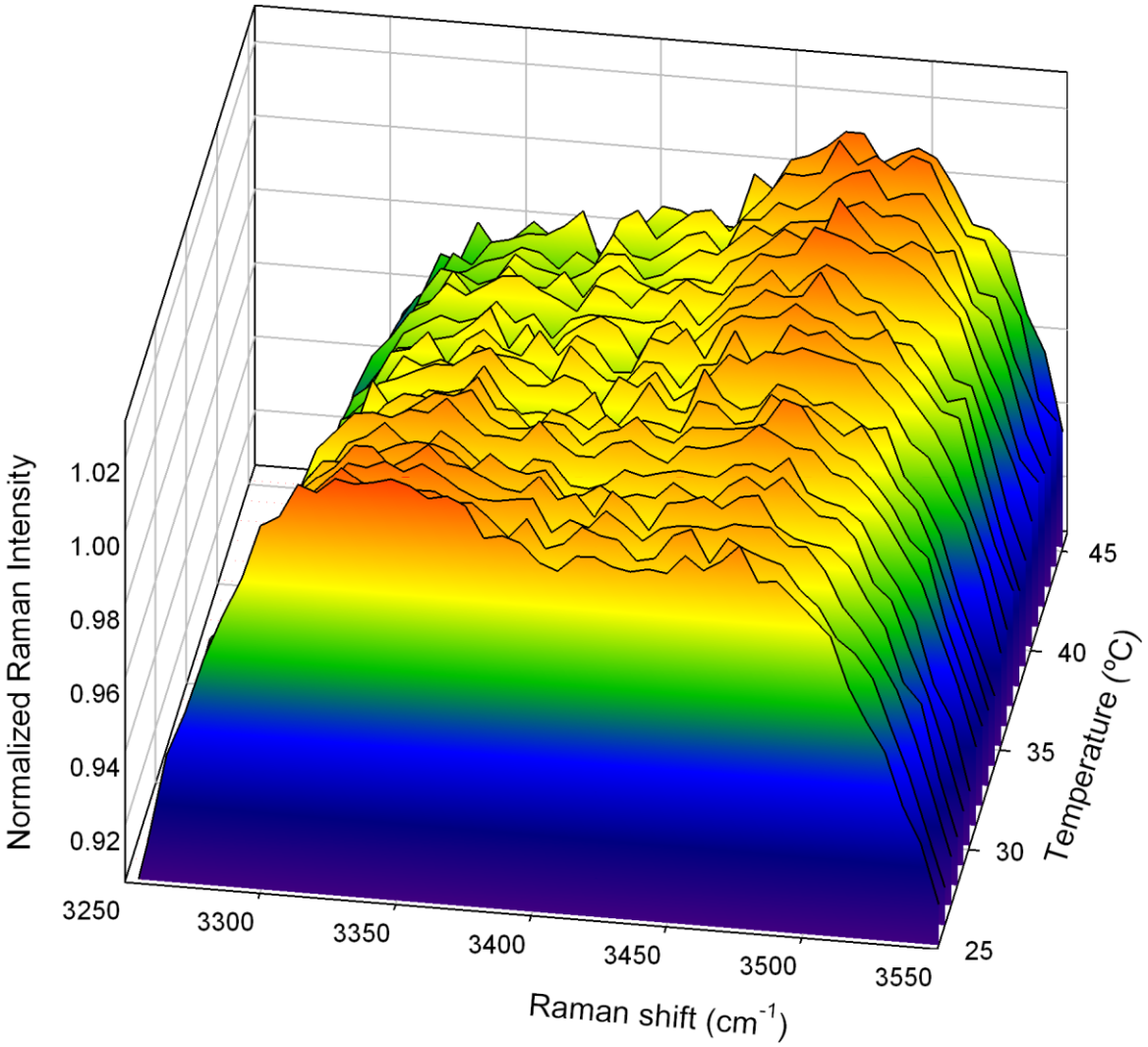
Normalized Raman Intensity
1.02
1.00
0.98
0.96
0.94
0.92
3250
3300
3350
3400
3450
3500
3550
Raman shift (cm-1)
25
30
35
40
45
Temperature (°C)

Fig. 9.

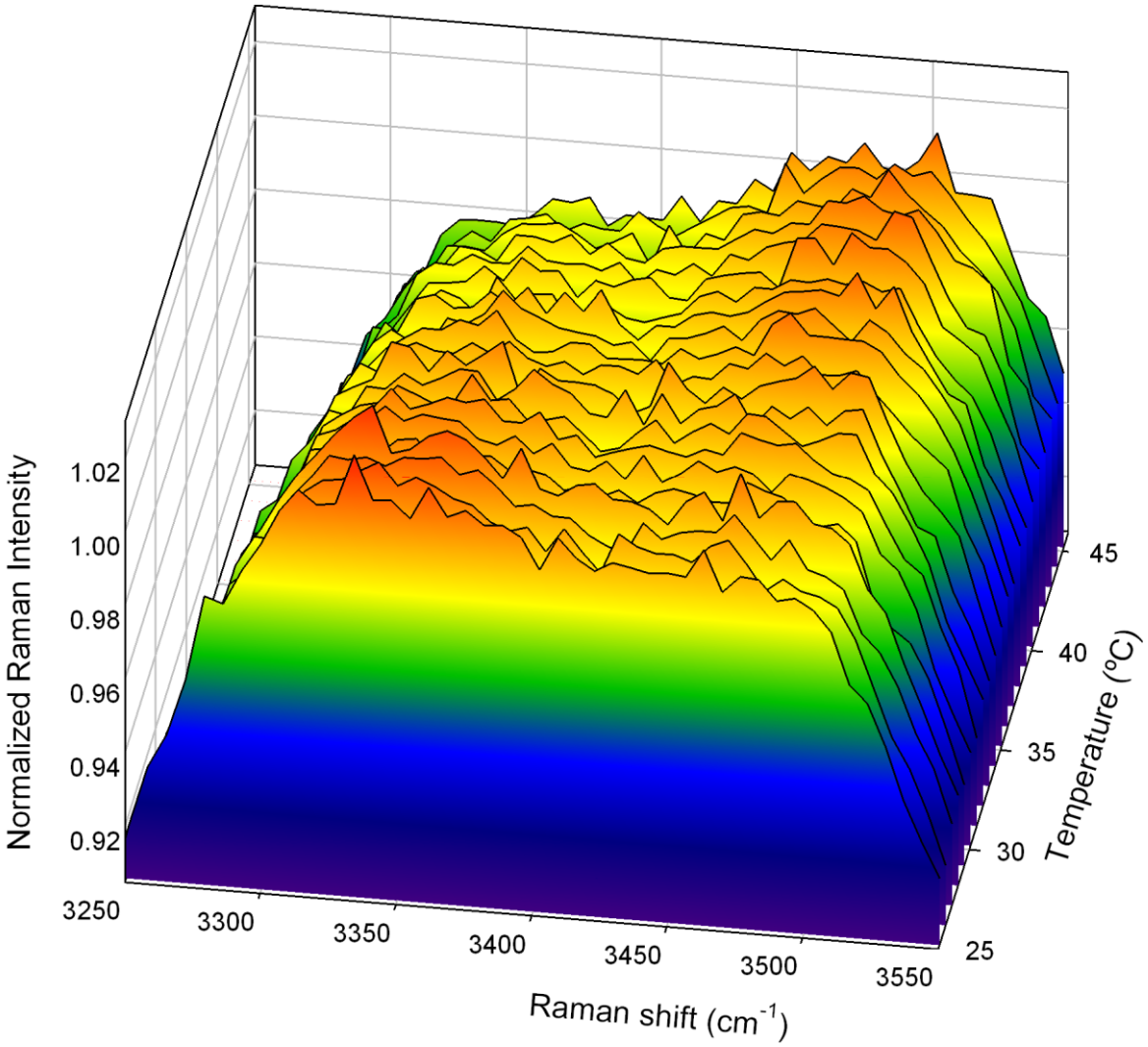
Normalized Raman Intensity
1.02
1.00
0.98
0.96
0.94
0.92
3250
3300
3350
3400
3450
3500
3550
Raman shift (cm-1)
25
30
35
40
45
Temperature (°C)

Fig. 10.

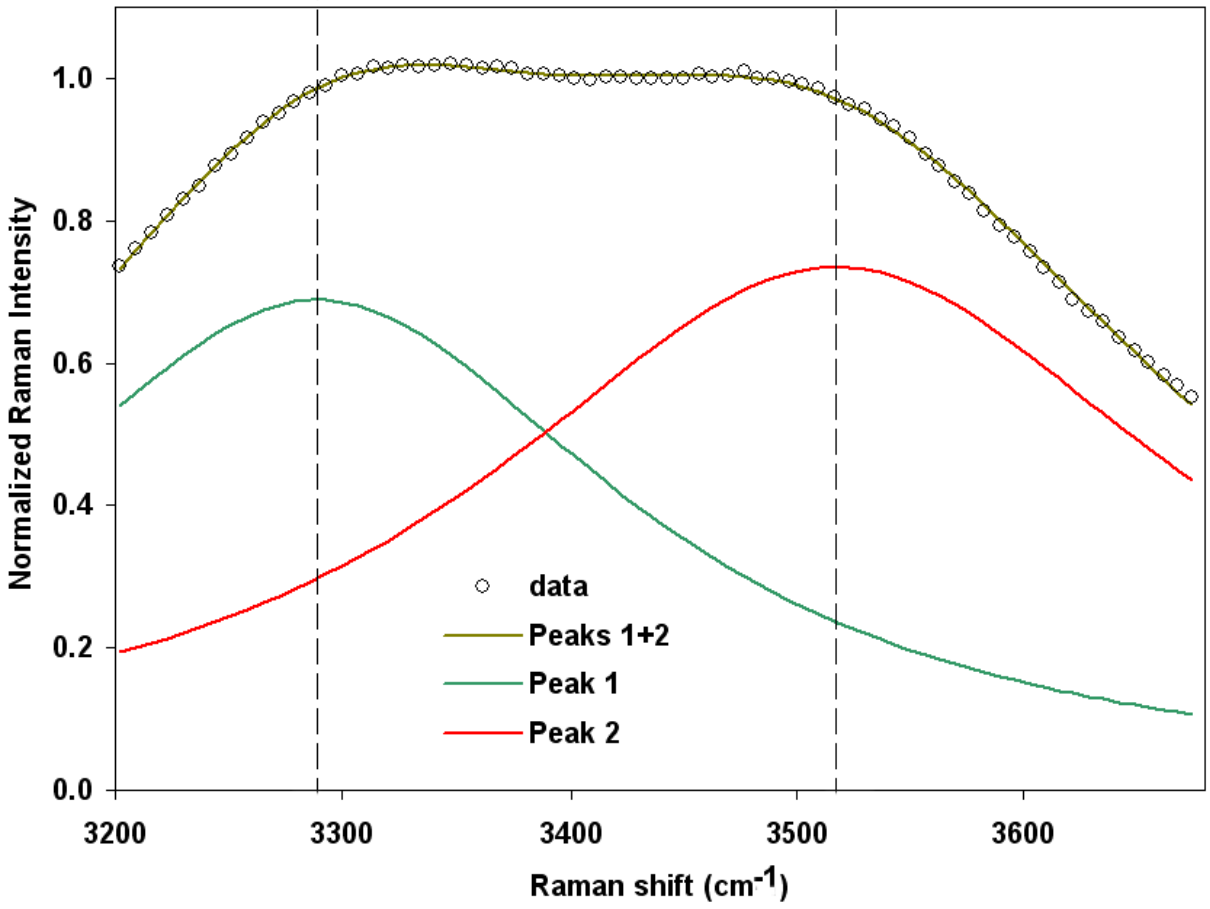
Normalized Raman Intensity
1.0
0.8
0.6
0.4
0.2
0.0
3200
3300
3400
3500
3600
Raman shift (cm-1)
data
Peaks 1+2
Peak 1
Peak 2

Fig. 11.

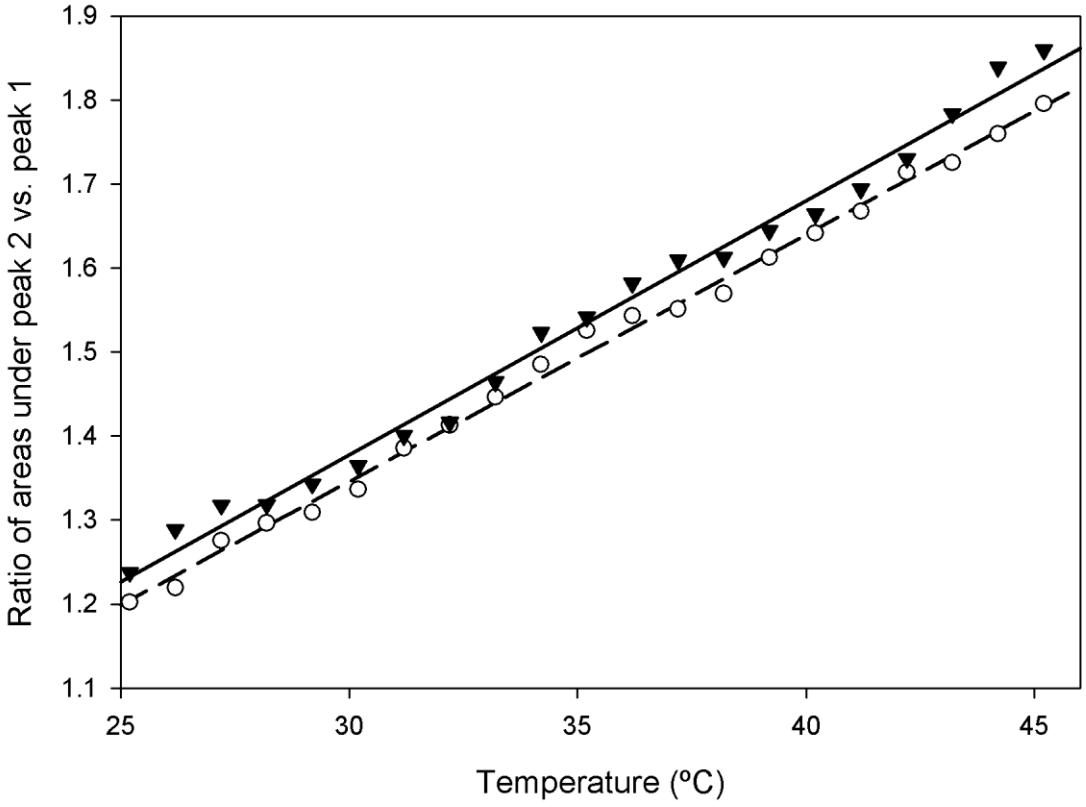
Ratio of areas under peak 2 vs. peak 1
1.9
1.8
1.7
1.6
1.5
1.4
1.3
1.2
1.1
25
30
35
40
45
Temperature (ºC)

Fig. 12

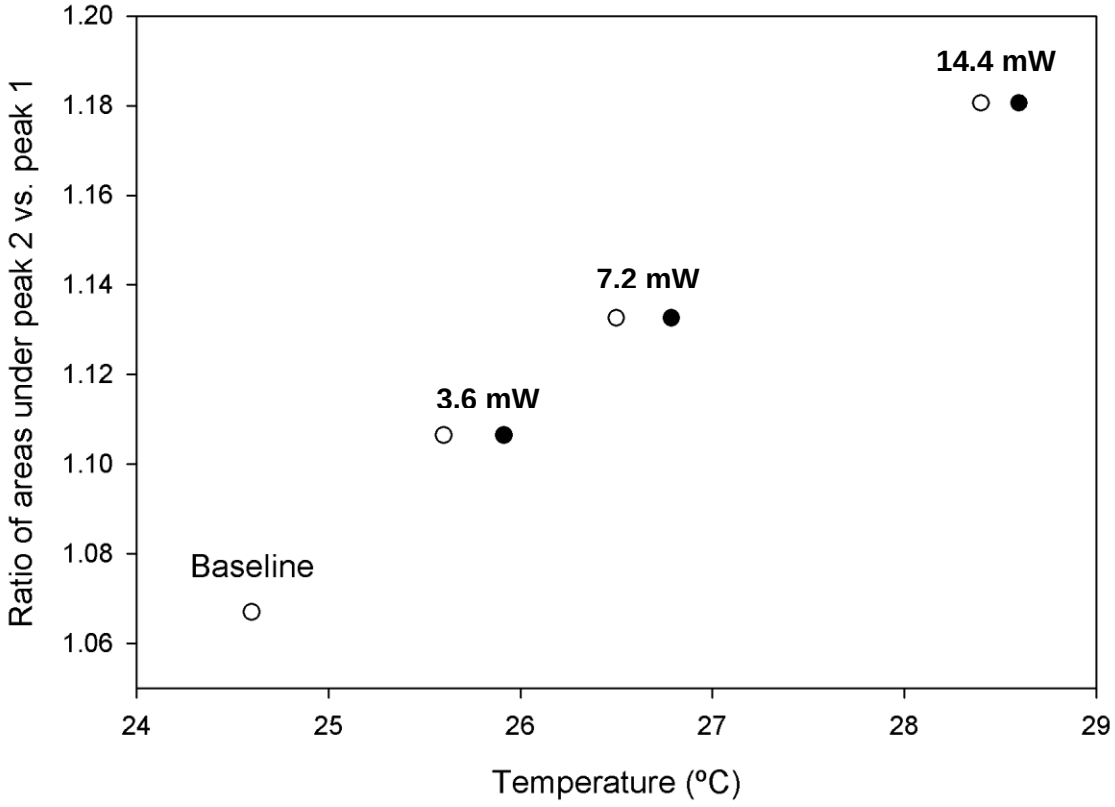
Ratio of areas under peak 2 vs. peak 1
1.20
1.18
1.16
1.14
1.12
1.10
1.08
1.06
24
25
26
27
28
29
Temperature (ºC)
14.4 mW
7.2 mW
3.6 mW
Baseline

Fig. 13.

Fig. S1. Supplemental Movie File